Novel Transformerless Grid-Connected Power Converter With Negative Grounding for Photovoltaic Generation System

Jia-Min Shen, *Student Member, IEEE*, Hurng-Liahng Jou, *Member, IEEE*, and Jinn-Chang Wu, *Member, IEEE*

***Abstract*—This paper proposes a novel transformerless grid-connected power converter with negative grounding for a photovoltaic generation system. The negative terminal of the solar cell array can be directly connected to the ground in the proposed grid-connected power converter to avoid the transparent conducting oxide corrosion that occurs in some types of thin-film solar cell array. The proposed grid-connected power converter consists of a dc–dc power converter and a dc–ac inverter. The salient features of the proposed power converter are that some power electronic switches are simultaneously used in both the dc–dc power converter and dc–ac inverter, and only two power electronic switches operate at high switching frequency at the same time (one is in the dc–dc power converter and the other is in the dc–ac inverter). The leakage current of the photovoltaic generation system is reduced because the negative terminal of the solar cell array is connected directly to the ground. Finally, a prototype was developed to verify the performance of the proposed grid-connected power converter. The experimental results show that the performance of the proposed grid-connected power converter is as expected.**

***Index Terms*—Leakage currents, solar power generation, thin films.**

I. Introduction

THE wide use of fossil fuels has resulted in the emission of greenhouse gases and the cost of fossil-fuel energy has become higher and higher. Climate change, caused by these greenhouse gases, has seriously damaged the environment. Because of the problems associated with climate change, interest in renewable energy sources, such as solar power and wind power, has increased [1]–[12].

Many materials can be used to manufacture solar cells, but polycrystalline Si and monocrystalline Si are the most widely used. A thin-film solar cell can generate power under conditions of low irradiation. Therefore, the thin-film solar cell has the potential to generate electrical power for a longer time than a crystalline Si solar cell. Since the thin-film cell can be easily combined with glass, plastic, and metal, it can be incorporated in green architecture. The use of thin-film solar cells has increased steadily and this trend is set to continue in the future.

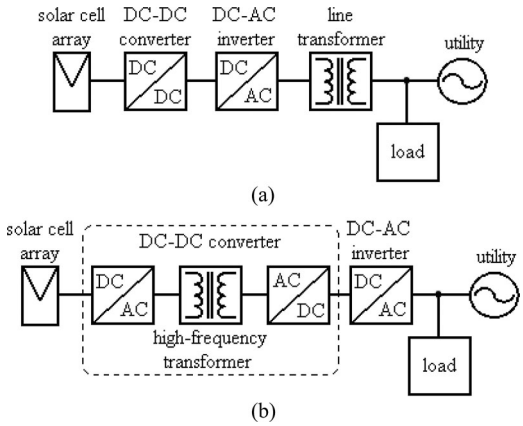

Fig. 1. Grid-connected photovoltaic generation system with an isolation transformer. (a) Line frequency transformer. (b) High-frequency transformer.

In general, an earth parasitic capacitance will be generated between solar modules and their ground. This parasitic capacitance is about 50–150 nF/kW for a glass-faced solar cell array [4], [13]. However, this capacitance is increased to 1 μF/kW if the thin-film solar cell array is used [4]. Serious leakage current occurs if a high-frequency pulsating voltage is applied between the thin-film solar modules and the ground [4], [14], [15]. Corrosion damage in thin-film modules, caused by a so-called transparent conductive oxide (TCO) corrosion of cadmium telluride (Cd-Te) or amorphous silicon (A-Si), is observed if the voltage of the negative terminal of a solar module is lower than that of the ground. The damage to the electrical conductivity of the inside of the glass cover cannot be repaired and causes substantial power loss [16]. Consequently, the life of thin-film solar modules is shortened [7], [17], [18]. However, TCO corrosion can be prevented by the negative grounding of solar modules.

Using an isolation transformer in the grid-connected inverter can solve the problem of the leakage current caused by the earth parasitic capacitance in solar modules. There are two types of grid-connected inverter with an isolation transformer. One is a line frequency transformer, and the other is a high-frequency transformer. Fig. 1(a) shows a grid-connected photovoltaic generation system with a line frequency transformer. The solar modules can be grounded directly and there is no current path for leakage current because the line frequency transformer is isolated [4], [19]. This system supplies no dc current to the grid and has the advantage of a simple control circuit. However, the

Manuscript received January 29, 2011; revised March 28, 2011 and June 1, 2011; accepted September 24, 2011. Date of current version February 20, 2012. Recommended for publication by Associate Editor J. M. Guerrero.

J.-M. Shen and H.-L. Jou are with the Department of Electrical Engineering, National Kaohsiung University of Applied Sciences, Kaohsiung 80778, Taiwan (e-mail: jiaminshen@gmail.com; hljou5519@gmail.com).

J.-C. Wu is with the Department of Microelectronics Engineering, National Kaohsiung Marine University, Kaohsiung 81143, Taiwan (e-mail: jinnwu@mail.nkmu.edu.tw).

Digital Object Identifier 10.1109/TPEL.2011.2170435

line frequency transformer's disadvantages are large volume, high weight, and high cost.

Fig. 1(b) shows a grid-connected photovoltaic generation system with a high frequency transformer. The transformer is incorporated in a dc–dc converter and is operated at high frequency to reduce volume and cost. However, the control circuit of this grid-connected photovoltaic generation system is complicated due to the use of a transformer-isolated dc–dc converter. Besides, the high-frequency transformer is not placed at the output of the grid-connected photovoltaic generation system, so it cannot prevent the dc current from injecting the grid.

The use of an isolation transformer in the grid-connected photovoltaic generation system should be avoided due to cost, size, and efficiency. In general, the bridge-type dc–ac inverter is used in the grid-connected photovoltaic generation system [15]. However, a conventional bridge-type dc–ac inverter, without an isolation transformer, results in the problem of leakage current because it cannot sustain the voltage of its negative terminal at a constant value. Recently, many dc–ac inverter topologies have been proposed to solve the problem of leakage current [7], [10], [14], [18], [20]–[23].

Lopez *et al*. proposed a diode-clamped multilevel dc–ac inverter [20]; Chen *et al*. proposed a hybrid diode-clamped multilevel dc–ac inverter [10]. In a multilevel dc–ac inverter, two split capacitors are connected to the dc bus of a dc–ac inverter and the middle point is connected to the neutral line of the utility. The two voltage terminals on the dc bus of a dc–ac inverter are clamped. No pulsating voltage is applied between the thin-film solar modules and the ground. So, the leakage current is suppressed. Ma *et al*. proposed Conergy neutral point clamped to simultaneously improve the efficiency of a diode-clamped multilevel inverter and overcome the leakage current problem [21]. Gonzalez *et al*. proposed the dc–ac inverter and Yu *et al*. proposed the H6 dc–ac inverter, in which one or two switches are combined with a full-bridge inverter to reduce the leakage current [14], [22]. Xiao *et al*. proposed several topologies to solve the problem of leakage current [23].

Although the aforementioned transformerless dc–ac inverter topologies can solve the leakage current problem, the negative grounding required in Cd-Te and A-Si thin-film solar cell array still cannot be solved. Boeke and van der Broeck proposed a three-phase four-wire dc–ac inverter with a split-capacitor arm where the middle point of the split-capacitor arm is connected to the neutral line of the three-phase four-wire distribution power system [7]. A buck-boost converter is used to build up the negative bus voltage. Araujo *et al*. proposed a novel grid-connected nonisolated converter with a grounded generator [18]. A novel dc–dc converter is applied to generate two dc capacitor voltages of the half-bridge dc–ac inverter where a transformer (coupling inductor) is integrated in the dc–dc converter to achieve the negative grounding of the solar cell array. The negative terminal of the solar cell array of the aforementioned two topologies can be directly connected to the ground, so the problems of leakage current and negative grounding are solved simultaneously.

This paper proposes a transformerless grid-connected power converter with negative grounding for a photovoltaic generation system. The proposed transformerless grid-connected power converter simultaneously solves the problems of leakage current and negative grounding as the topologies shown in [7] and [18]. The negative grounding of the solar cell array in the proposed paper is achieved by a boost dc–dc converter and select switches. Therefore, the problem of TCO corrosion in Cd-Te or A-Si thin-film solar modules is also solved. Finally, a prototype was developed and tested to verify the performance of the proposed transformerless photovoltaic generation system.

II. Leakage Current of a DC–AC Inverter

This section analyzes and discusses the problem of leakage current in a grid-connected photovoltaic generation system that uses a conventional half-bridge inverter, a conventional full-bridge inverter, and a diode-clamped multilevel half-bridge inverter. Fig. 2 shows the relevant circuit configurations. In the following analysis, the capacity of the solar cell array shown in Fig. 2 is assumed to be 1 kW. An equivalent capacitor C_p is serially connected to an equivalent resistor R_{g1} to represent the parasitic elements of the solar cell array, and these are connected between the negative terminal of the solar cell array and the ground. The utility is connected to the ground by an equivalent resistor R_{g2}. The capacitance of the parasitic capacitor C_p is typically 1 μF in a 1-kW solar cell array. Since the utility voltage is 120 V, R_{g2} must be lower than 25 Ω to satisfy the requirements [24]. Fig. 2(a) shows a conventional half-bridge inverter, which is controlled by pulsewidth modulation (PWM) and named as type 1. Fig. 2(b) shows a conventional full-bridge inverter. The conventional full-bridge inverter can be controlled by a bipolar PWM or a unipolar PWM, named as type 2 and type 3, respectively. Fig. 2(c) shows the diode-clamped multilevel half-bridge inverter named as type 4. A filter inductor L_f connected to the output of the dc–ac inverter is used for filtering the switching harmonic of the dc–ac inverter.

Table I shows the main parameters of the simulation system. Fig. 3 shows the simulation results for the resistors $R_{g1} = 1\ \Omega$ and $R_{g2} = 1\ \Omega$. As can be seen, the grounding voltage v_g and the leakage current i_g differ for different types of dc–ac inverters. For the conventional half-bridge and diode-clamped multilevel half-bridge inverters (type 1 and type 4), the neutral line of the utility is directly connected to the middle point of the split dc capacitors. The voltage between the negative terminal of the solar cell array and the ground is stabilized by the lower dc capacitor of these types of dc–ac inverters. As seen in Fig. 3, the voltage of the negative terminal for these types of dc–ac inverters is -200 V. A voltage ripple with a frequency equaling that of the utility is incorporated in the voltage of the negative terminal because the ac current connected to the utility passes through the split dc capacitors. This voltage ripple is very small and depends on the capacitance of the split dc capacitors. Since the impedance of the earth parasitic capacitance is very large at the utility frequency, the leakage current of the utility frequency is very small. Fig. 3 shows a small high-frequency leakage current in the half-bridge inverter. This is due to the equivalent ground resistor R_{g2} of the utility and switching operation of the power electronic switches. However, the leakage current for the half-bridge inverter is less than 2.5 mA.

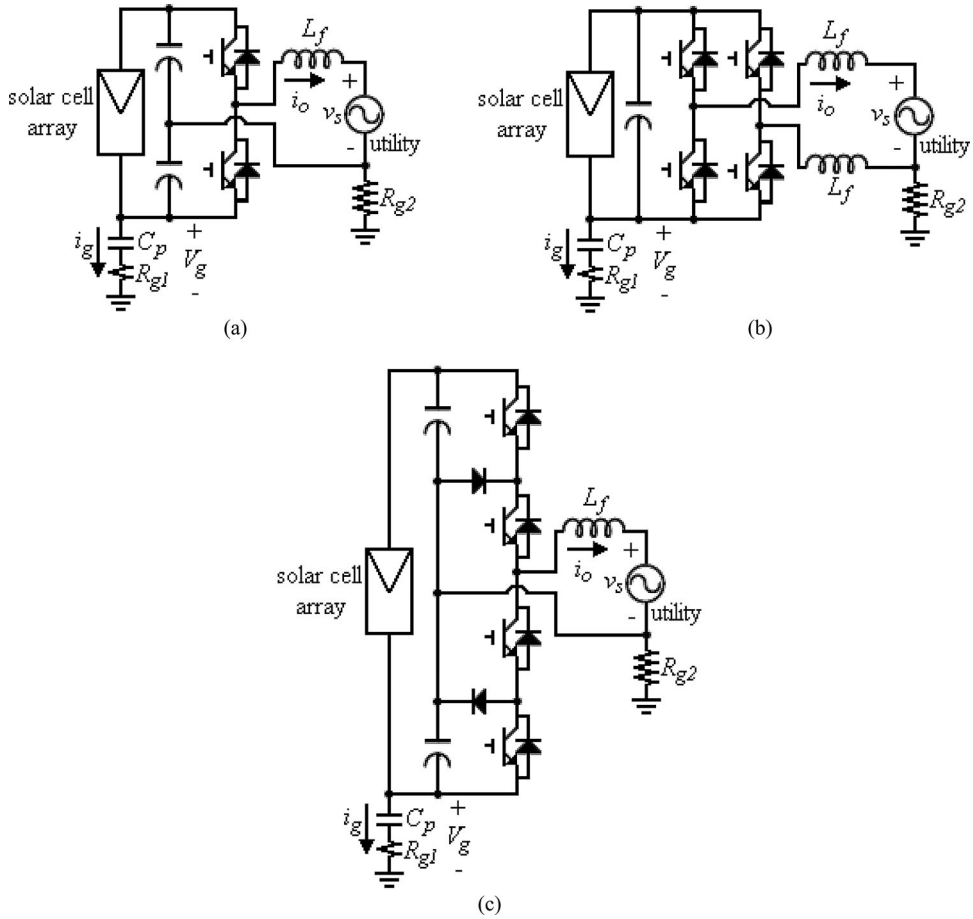

Fig. 2. Inverter topologies used in the grid-connected photovoltaic generation system. (a) Conventional half-bridge inverter. (b) Conventional full-bridge inverter. (c) Diode-clamped multilevel half-bridge inverter.

TABLE I
MAIN PARAMETERS FOR DIFFERENT INVERTERS USED IN THE SIMULATION

Parameters	Value
C_p	1μF
f_{sw}	20kHz
L_f (type 1)	3mH
L_f (type 2)	1.5mH×2
L_f (type 3)	1mH×2
L_f (type 4)	2mH

During the positive half-cycle of the utility voltage, the switching operation occurs at the upper side of the diode-clamped multilevel half-bridge inverter and results in a switching ripple in the upper side capacitor. However, the voltage of the lower side capacitor is sustained and no leakage current is generated between the negative terminal and the ground. Similarly, this switching ripple will appear in the lower side capacitor during the negative half-cycle of the utility voltage and result in a small leakage current between the negative terminal and the ground. However, the leakage current for the diode-clamped multilevel half-bridge inverter is still less than 2 mA.

As seen in Fig. 2(b), the two lines from the utility are connected to the midpoints of two power electronic switch legs of a conventional full-bridge dc–ac inverter. To achieve symmetrical circuit configuration and better suppress the leakage current, two filter inductors are connected between the outputs of the dc–ac inverter and the utility, respectively. As can be seen in Fig. 3, the voltage at the negative terminal of type 2 is a voltage ripple with a dc offset. The amplitude, frequency, and dc offset are 90 V, 60 Hz, and −100 V, respectively. The voltage at the negative terminal of type 2 contains no pulsating voltage at the switching frequency due to the symmetric switching of the bipolar PWM. Since this voltage ripple is low frequency, the peak value of the leakage current is smaller than 50 mA. However, this leakage current is larger than that of the conventional half-bridge and the diode-clamped multilevel half-bridge inverters.

Fig. 3 also shows that the voltage at the negative terminal of type 3 contains a pulsating voltage with a frequency equaling the switching frequency due to the asymmetric switching of the unipolar PWM. The magnitude of this pulsating voltage is 90 V and results in a serious leakage current (about 1A) through the parasitic capacitance of the solar cell array.

Fig. 4 shows the simulation results for resistors $R_{g1} = 10\ \Omega$ and $R_{g2} = 10\ \Omega$. As can be seen, the simulation results are similar to those of Fig. 3. From the simulation results shown in Figs. 3 and 4, it can be seen that the leakage current in the conventional full-bridge inverter controlled by the unipolar PWM is too large to comply with the standard VDE 0126-1-1 [25].

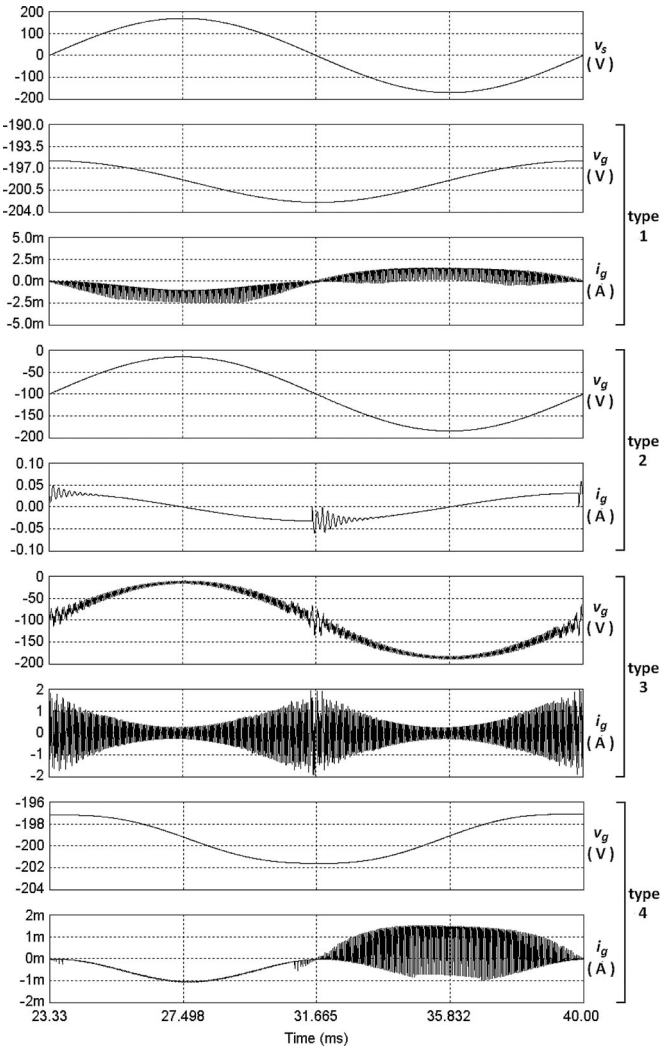

Fig. 3. Simulation results for different types of inverter under 1 μF, $R_{g1} = 1\ \Omega$, and $R_{g2} = 1\ \Omega$.

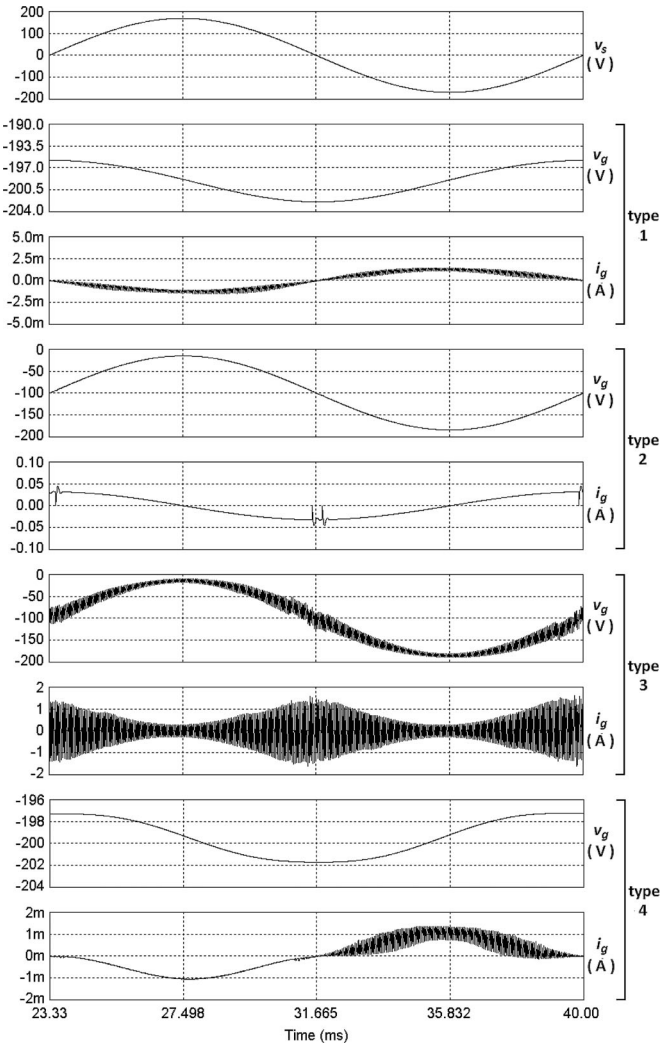

Fig. 4. Simulation results for different types of inverter under 1 μF, $R_{g1} = 10\ \Omega$, and $R_{g2} = 10\ \Omega$.

The major reason for grounding connection is safety. In practical applications, the grounding resistance is usually very small. The earth parasitic capacitance, between the solar cell array and the ground, will cause leakage current and result in additional power loss. Table II shows the calculated power loss caused by the leakage current for the same earth parasitic capacitance (1 μF) and different resistors R_{g1} and R_{g2} (1 Ω, 5 Ω, and 10 Ω) in a 1-kW solar cell array [10], [26]. The power loss is the product of the square of the leakage current and the summation of equivalent resistors R_{g1} and R_{g2}. As can be seen in Table II, the leakage currents are small in the conventional half-bridge inverter, the conventional full-bridge inverter with bipolar PWM, and the diode-clamped multilevel half-bridge inverter. As seen in Table II, the power loss caused by the leakage current in types 1, 2, and 4 is very small. However, the power loss caused by the leakage current is significant in type 3, and it will evidently degrade the system efficiency. Besides, it can also be found that the calculated power loss of type 3 increases as the resistance is increased. Additionally, the leakage current will cause additional power loss at the filter inductor and power electronic switches. The power loss caused by the leakage current of type 3 will be higher than 1% in practice after considering the effects of both the parasitic and nonparasitic components.

III. Circuit Configuration

Fig. 5 shows the circuit configuration of the proposed photovoltaic generation system. As can be seen, the grid-connected power converter is transformerless, and its negative terminal is connected directly to the ground. Both the problems of TCO corrosion and leakage current in Cd-Te or A-Si thin-film solar cell array can be avoided. The proposed transformerless grid-connected power converter is composed of a dc–dc power converter and a dc–ac inverter. The dc–dc power converter is a boost converter. The dc–dc power converter consists of three dc capacitors C_1, C_2, and C_3, an inductor L_1, two diodes D_1 and D_2, and four power electronic switches G_1, G_2, G_3, and G_5. The dc–dc power converter converts the dc voltage of the solar cell array to a stabilized dc voltage. The dc–ac inverter consists of two dc capacitors C_2 and C_3, an ac inductor L_f, and four

TABLE II
CALCULATED POWER LOSS CAUSED BY THE LEAKAGE CURRENT UNDER DIFFERENT R_{g1} AND R_{g2} IN 1-KW THIN-FILM SOLAR MODULES

Type	R_{g1}=1Ω R_{g2}=1Ω		R_{g1}=5Ω R_{g2}=5Ω		R_{g1}=10Ω R_{g2}=10Ω	
	Power loss (W)	%	Power loss (W)	%	Power loss (W)	%
Type 1	1.2m	ignore	1.8m	ignore	1.2m	ignore
Type 2	2.7m	ignore	7.5m	ignore	11.8m	ignore
Type 3	1.2	0.12	4.3	0.43	7.7	0.77
Type 4	0.9m	ignore	0.9m	ignore	0.8m	ignore

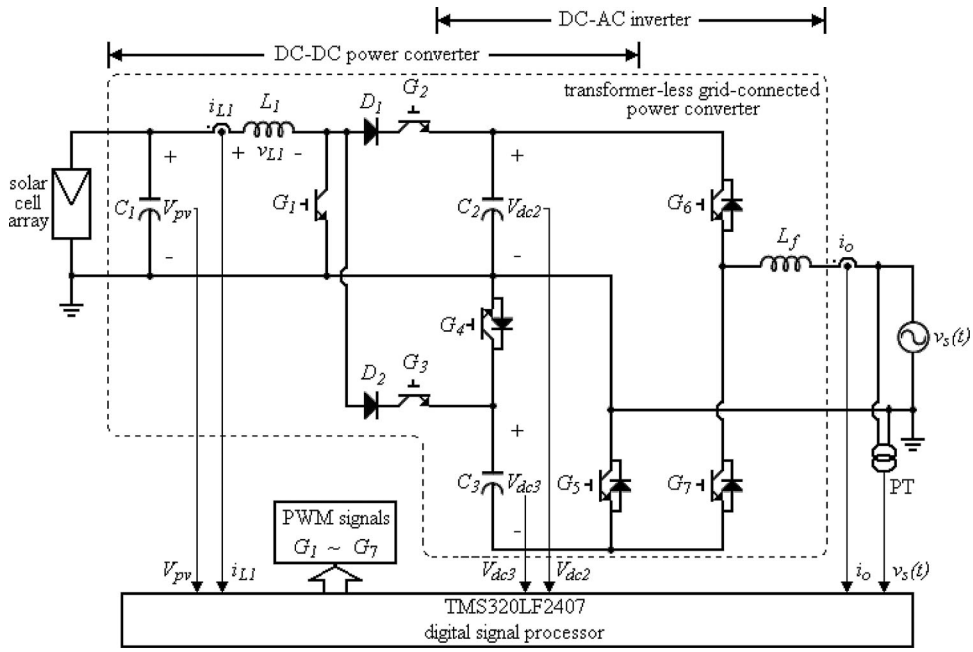

Fig. 5. Circuit configuration of the proposed transformerless negative grounding photovoltaic generation system.

power electronic switches G_4, G_5, G_6, and G_7. The dc–ac inverter further converts the output dc voltage of the dc–dc power converter into ac power and injects into the grid. As seen in Fig. 5, the power electronic switch G_5 controls both the dc–dc power converter and the dc–ac inverter.

IV. OPERATING PRINCIPLE OF THE PROPOSED POWER CONVERTER

Fig. 6 shows the switching pattern for the power electronic switches of the proposed transformerless grid-connected power converter. As can be seen, (G_2, G_7) and (G_3, G_5) are switched in opposition and synchronous with the utility voltage, respectively. G_1 is switched at high frequency to store or release the energy in the inductor L_1, and then regulate the output voltage of the dc–dc power converter. G_6 and G_4 are, respectively, switched at high frequency during the positive half-cycle and the negative half-cycle of the utility voltage to control the output current of the dc–ac inverter. Since only one power electronic switch in the dc–ac inverter is switched at high frequency, the power loss caused by the switching operation is reduced.

Fig. 7 shows the timing sequence for power electronic switches of the proposed power converter. Fig. 7(a) is the timing sequence for power electronic switches during the positive half-cycle of the utility voltage. During the positive half-cycle of the utility voltage, the dc–dc power converter charges

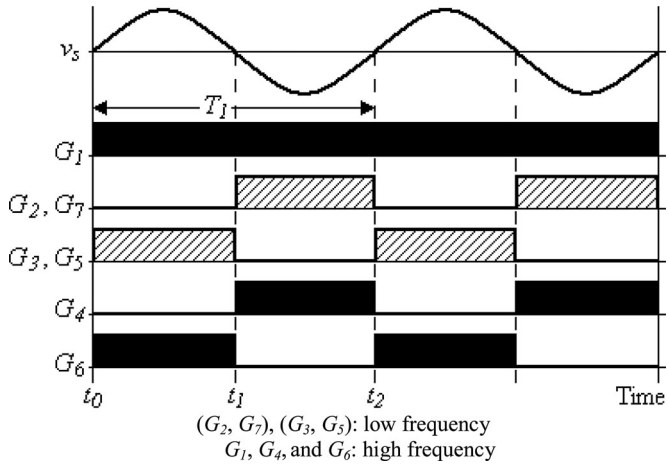

Fig. 6. Switching pattern for the power electronic switches of the proposed transformerless negative grounding photovoltaic generation system. (G_2, G_7), (G_3, G_5): low frequency. G_1, G_4, and G_6: high frequency.

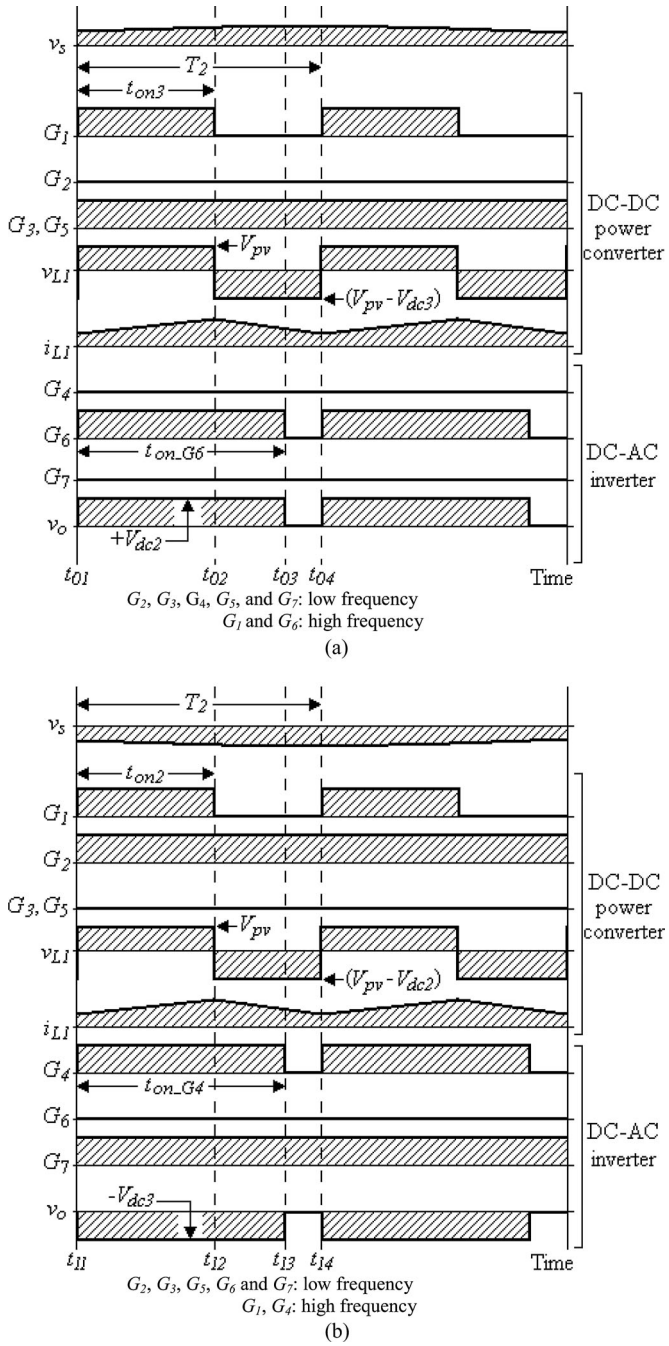

Fig. 7. Timing sequence for power electronic switches of the proposed power converter. (a) Positive half-cycle. G_2, G_3, G_4, G_5, and G_7: low frequency, G_1 and G_6: high frequency. (b) Negative half-cycle. G_2, G_3, G_5, G_6 and G_7: low frequency, G_1, G_4: high frequency.

capacitor C_3 so the duty cycle ($D_{u3} = t_{\rm on3}/T_2$) of G_1 controls the voltage of capacitor C_3. The capacitor C_2 supplies power to the dc–ac inverter, and G_6 of the dc-ac inverter is switched at high frequency to control the output current. As seen in Fig. 7(a), the operation of power electronic switches during the positive half-cycle can be divided into three time intervals. The current paths, during these time intervals, are shown in Fig. 8 and described as

1) $[t_{01}, t_{02}]$
The current path during this time interval is shown in Fig. 8(a). G_1 of the dc–dc power converter is switched on to energize the inductor L_1. Because G_3 and G_5 are both ON, a diode D_2 is series connected to G_3 to prevent C_3 from short circuit. In the dc–ac inverter, G_6 is switched ON and the output voltage v_o is $+V_{\rm dc2}$. The output current of the dc–ac inverter is supplied from C_2.
2) $[t_{02}, t_{03}]$
The current path during this time interval is shown in Fig. 8(b). In the dc–dc power converter, G_1 and G_2 are switched OFF. G_3 and G_5 are still ON. The energy stored in the inductor L_1 is deenergized via the path D_2, G_3 and the flying diode of G_5 to charge the capacitor C_3. G_6 of the dc–ac inverter is still ON, and the output voltage v_o is still $+V_{\rm dc2}$. The filter inductor of the dc–ac inverter is energized from C_2.
3) $[t_{03}, t_{04}]$
The current path during this time interval is shown in Fig. 8(c). In the dc–dc power converter, the energy stored in the inductor L_1 is still deenergized via the path D_2, G_3 and the flying diode of G_5 to charge the capacitor C_3. G_6 of the dc–ac inverter is switched OFF, and the output current is flowing through G_5 and the flying diode of G_7 to form a loop. Therefore, the voltage v_o is 0, and the filter inductor of the dc–ac inverter is deenergized.

Fig. 7(b) shows the timing sequence for power electronic switches during the negative half-cycle of the utility voltage. For the negative half-cycle of the utility voltage, the dc–dc power converter charges the capacitor C_2, so the duty cycle ($D_{u2} = t_{\rm on2}/T_2$) of G_1 controls the voltage of capacitor C_2. Capacitor C_3 supplies power to the dc–ac inverter, and G_4 of the dc–ac inverter is switched at high frequency to control the output current. As seen in Fig. 7(b), the operation of power electronic switches during the negative half-cycle of the utility voltage can also be divided into three time intervals. The current paths during these time intervals of the negative half-cycle of the utility voltage are shown in Fig. 8(d)–(f). Because the operation of the negative half-cycle of the utility voltage is similar to that of the positive half-cycle, its explanation is superfluous.

V. Control Block

Fig. 9 shows the control block diagram for the proposed transformerless grid-connected power converter. Fig. 9(a) is the control block diagram for the dc–dc power converter. G_1 of the dc–dc power converter controls the dc voltages of C_2 and C_3. As already mentioned, the positive and the negative half-cycles of the ac current are alternately supplied from the dc capacitors C_2 and C_3, and the dc capacitors C_2 and C_3 are individually charged during different half-cycles. Therefore, the dc voltages of C_2 and C_3 will contain a voltage ripple with a frequency equaling the utility frequency. The generating power of the solar cell array will decrease if their output voltage contains a voltage ripple. To avoid the voltage ripple delivered from the dc capacitors C_2 and C_3 to the solar cell array, the current in the inductor L_1

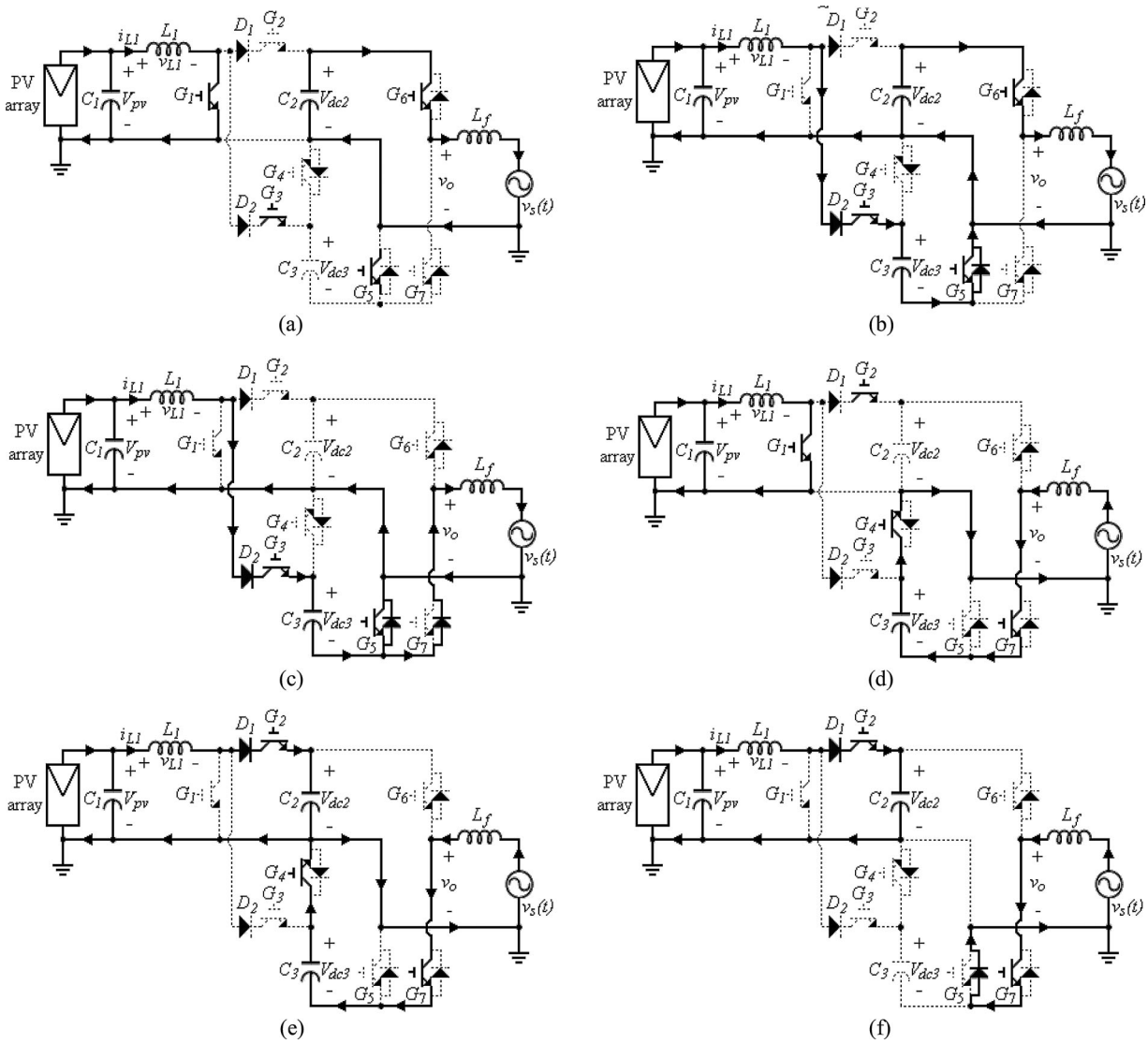

Fig. 8. Current path under different time duration. (a) $[t_{01}, t_{02}]$. (b) $[t_{02}, t_{03}]$. (c) $[t_{03}, t_{04}]$. (d) $[t_{11}, t_{12}]$. (e) $[t_{12}, t_{13}]$. (f) $[t_{13}, t_{14}]$.

must be ripple free. Consequently, the dc–dc power converter is controlled by an outer voltage loop and an inner current loop.

As mentioned previously, C_2 and C_3 are, respectively, charged by the dc–dc power converter in the negative and the positive half-cycles of the utility. As seen in Fig. 9(a), the capacitor voltages $V_{\rm dc2}$ and $V_{\rm dc3}$ are detected and sent to band-stop filters I and II, respectively. The band-stop filters I and II are used to eliminate the utility frequency ripple. The outputs of the band-stop filters I and II are subtracted from a setting capacitor voltage $V_{\rm dc\_set}$, and then the results are sent to the proportional-integral (PI) controllers I and II to generate the reference current signal, respectively. A switch is used to select the outputs of the PI controllers I and II to synchronize with the utility. In the positive half-cycle of the utility, the output of the PI controller II is selected. On the contrary, the output of the PI controller I is selected in the negative half-cycle of the utility. The output of the switch is a reference current signal. Since the capacitor voltages $V_{\rm dc2}$ and $V_{\rm dc3}$ are controlled by the individual half-cycle and individual PI controller, the voltages of C_2 and C_3 can be balanced. The reference current signal and the detected inductor current are sent to a subtractor, and then the result is sent to an amplifier. The output of the amplifier is sent to a PWM circuit, and the output of the PWM circuit is sent to a driving circuit to generate the driving signal for G_1.

Fig. 9(b) shows the control block diagram for the dc–ac inverter. The utility voltage is detected and fed to a phase-locked loop (PLL) circuit to generate a unity sinusoidal signal in phase with the utility voltage. This unity sinusoidal signal is sent to a comparator to generate a square wave S_1 whose phase is the same as the utility. The output signal of the comparator is sent to a driving circuit to generate the driving signals for G_3 and G_5. The output signal of the comparator is also sent to a signal inverter. The output signal S_2 of the signal inverter, which is out of phase with the utility voltage, is sent to a driving circuit to generate the driving signals for G_2 and G_7.

The maximum power point tracking (MPPT) method used in this paper is modified from that used in a small wind-power generation system [27]. The function of MPPT can be obtained

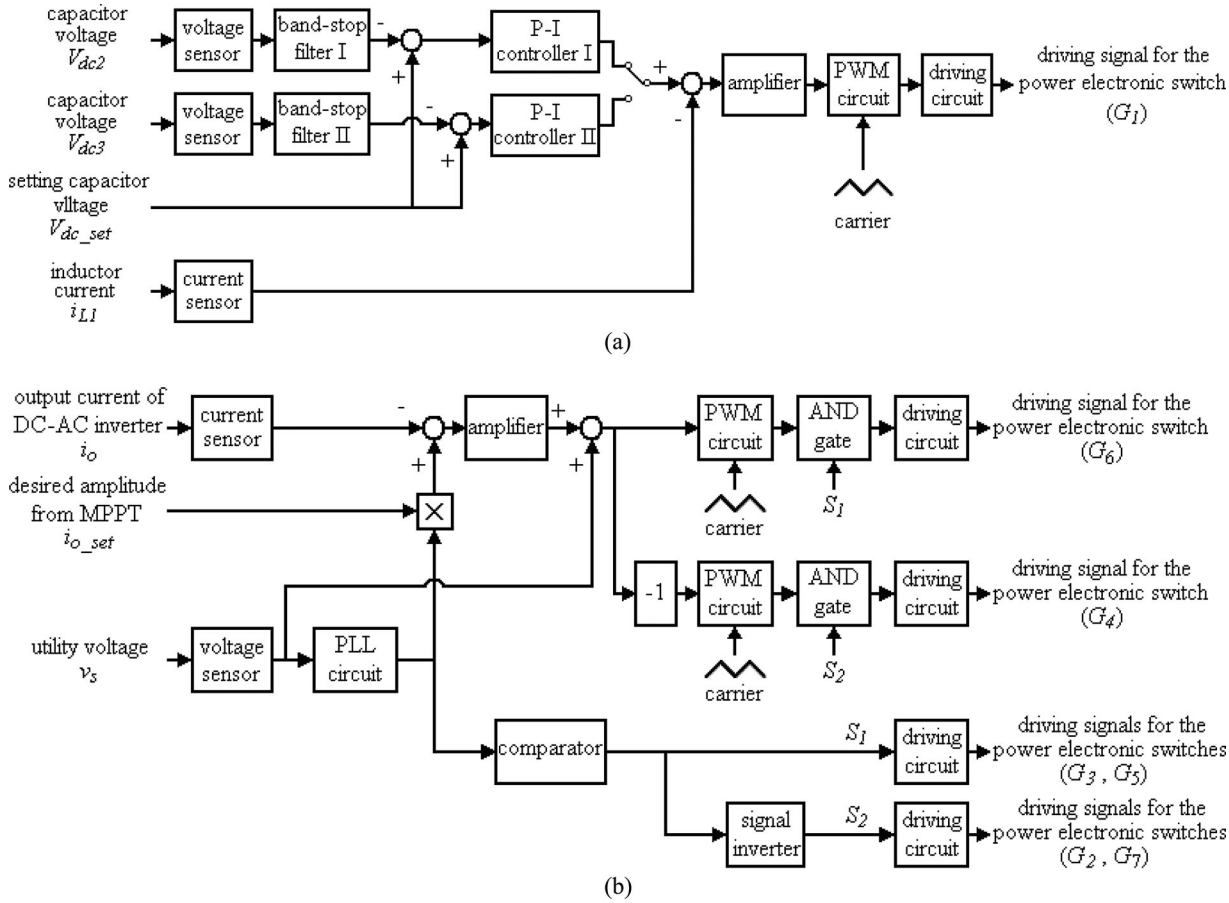

Fig. 9. Control block of the proposed transformerless grid-connected power converter. (a) DC–DC power converter. (b) DC–AC inverter.

by perturbing the amplitude of the output current of the dc–ac inverter, and then observing the voltage variation of the solar cell array to determine the next perturbation direction for the amplitude of the output current of the dc–ac inverter. The output of the MPPT control block is an amplitude signal. The outputs of the PLL circuit and the MPPT control block are sent to a multiplier to provide a reference output current for the dc–ac inverter. The reference output current and the detected output current of a dc–ac inverter are sent to a subtractor, and the result is then sent to an amplifier. The output of the amplifier and the detected utility voltage is sent to an adder. To avoid interference from the utility voltage, a feedforward control is used, and it is obtained by adding the detected utility voltage. The output of the accumulator is sent to a PWM circuit. The output of the PWM circuit and the signal S_1 are sent to an AND gate, and then sent to a driving circuit to generate a driving signal for G_6. This means G_6 is operated at a high switching frequency during the positive half-cycle of the utility voltage.

The output of the amplifier is also sent to an inverting amplifier. The output of this inverting amplifier is sent to a PWM circuit. The output of the PWM circuit and the signal S_2 are sent to an AND gate, and then sent to a driving circuit to generate a driving signal for G_4. This means G_4 is operated at a high switching frequency during the negative half-cycle of utility voltage. Note, only one power electronic switch in the dc–ac inverter is operated at a high switching frequency.

Since the operation principle of the proposed dc–ac inverter in the positive and the negative half-cycles of the utility is the same, only the positive half-cycle of the utility is discussed in deriving the model of the proposed dc–ac inverter. If the output signal v_m of the amplifier is constant in a switching period, the duty ratio of the single-phase converter can be represented as [28]

$$d = \frac{v_m}{\hat{V}_{\rm tri}} \tag{1}$$

where $\hat{V}_{\rm tri}$ is the amplitude of the high-frequency carrier. The equations of the dc–ac inverter can be obtained as

$$L\frac{di_o}{dt} = v_o - v_s \tag{2}$$

where v_o and i_o are the output voltage and output current of the dc–ac inverter, respectively, and v_s is the utility voltage. If the high frequency harmonic due to the PWM switching can be filtered out effectively, the average output voltage of the dc–ac inverter can be represented as

$$v_o = d_x V_{\rm dc} = k_{\rm pwm} v_m \tag{3}$$

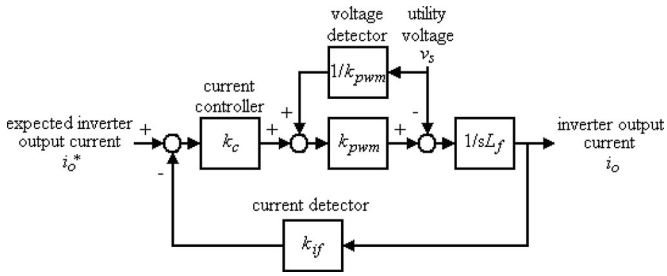

Fig. 10. Simplified model of the dc–ac inverter.

where $k_{\rm pwm} = V_{\rm dc}/\hat{V}_{\rm tri}$. Since the output power is supplied from C_2 in the positive half-cycle of the utility, $V_{\rm dc}$ is the voltage $V_{\rm dc2}$. Consequently, $V_{\rm dc}$ is the voltage $V_{\rm dc3}$ in the negative half-cycle of the utility. The model of the dc–ac inverter with the current mode control is shown in Fig. 10, where k_{if} is the gain of the current detector. As seen in Fig. 10, the feedforward control of the utility is also incorporated into the controller, and the gain of the feedforward control is $1/k_{\rm pwm}$. Therefore, the interference of the utility voltage can be avoided by the feedforward control. The current controller is an amplifier with gain k_c. The closed-loop transfer function of the current loop can be represented as

$$\frac{i_o}{i_o^*} = \frac{k_{\rm pwm}k_c}{sL_f + k_{if}k_{\rm pwm}k_c}. \tag{4}$$

As seen in (4), the dc–ac inverter is a first-order system. The gain k_c of the amplifier determines the bandwidth of the dc–ac inverter. The bandwidth of the dc–ac inverter is limited by the switching frequency. Since the high switching frequency is used in the low capacity dc–ac inverter, a high gain of current controller is designed to avoid the steady-state error and to obtain quick response. Besides, the feedforward control of the utility is also incorporated into the controller of the dc–ac inverter. So, the steady-state error can be further reduced. Therefore, the proportional controller is used as the current controller to simplify the control circuit of the dc–ac inverter.

VI. Experimental Results

A prototype was developed to verify the performance of the proposed transformerless grid-connected power converter. The power electronic switches G_1 –G_7 used in this paper are insulated gate bipolar transistor modules CM100DY-12H, and the power diodes D_1 and D_2 are RHRG30120. The controllers of the dc–dc power converter and the dc–ac inverter are implemented in a DSP of TMS320LF2407. The major parameters of the prototype are listed in Table III. The solar cell array is configured in two strings. Each string contains nine solar modules connected in series.

Fig. 11 shows the experimental results for the characteristics of the solar cell array. The environmental temperature and the radiation levels are 25.0 °C and 916.4 W/m^2, respectively. The temperature of the solar module is 46.7 °C. The maximum output power of the solar cell array is about 931 W. Fig. 12 shows the experimental results for the MPPT performance of the proposed grid-connected power converter. The MPPT controller was agitated every 1.2 s. As seen in Fig. 12, the output power of the solar cell array in the proposed grid-connected power converter is around 931 W. Therefore, the proposed grid-connected power converter can track the maximum power point effectively.

Fig. 13 shows the experimental results for the dc–ac inverter of the proposed transformerless grid-connected power converter under the steady state. The output power of the solar cell array

TABLE III
Major Parameters of the Prototype

Solar Module	
Model	F-MSN-75W-R-02
Rate of maximum power	75W
Open voltage	21.7V
Short current	5.0A
system parameter	
Utility voltage	120V, 60Hz
Switch frequency	18kHz
DC capacitor (C_1)	470μF
DC bus capacitor (C_2)	1,680μF
DC bus capacitor (C_3)	1,680μF
DC inductor (L_1)	2.8mH
AC inductor (L_f)	2.8mH

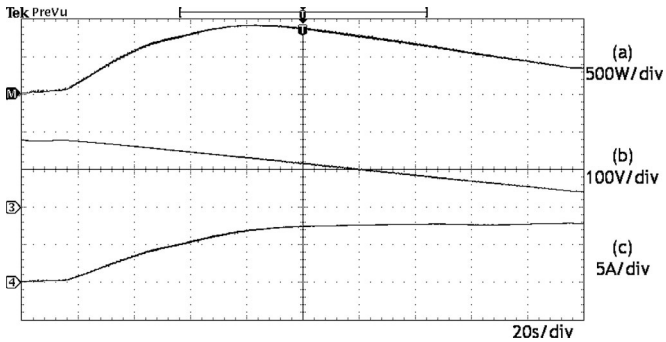

Fig. 11. Experimental results for the characteristics of the solar cell array. (a) Output power. (b) Voltage of the solar cell array. (c) Current of the solar cell array.

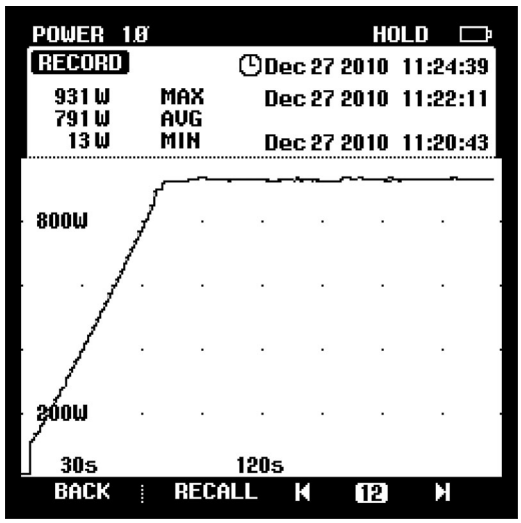

Fig. 12. Experimental results for the MPPT performance of the proposed grid-connected power converter.

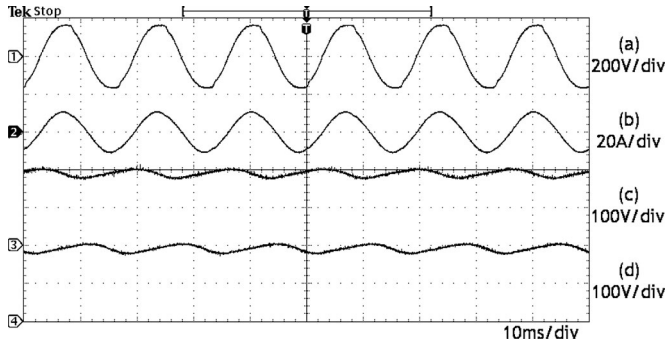

Fig. 13. Experimental results of the dc–ac inverter for the proposed transformerless grid-connected power converter under the steady state. (a) Utility voltage. (b) Output current of the dc–ac inverter. (c) Capacitor voltage V_{dc2}. (d) Capacitor voltage V_{dc3}.

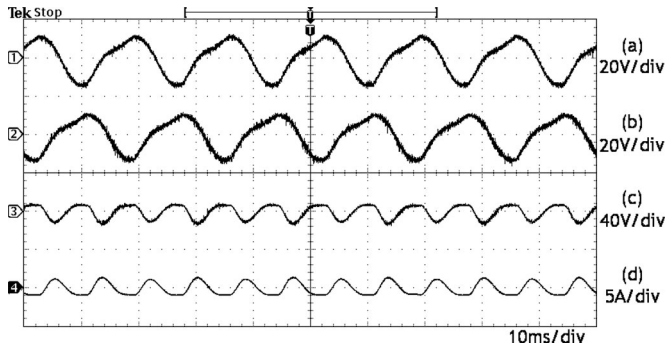

Fig. 14. Experimental results of the dc–dc power converter using a conventional voltage controller. (a) Voltage ripple of capacitor C_2. (b) Voltage ripple of capacitor C_3. (c) Output voltage ripple of the solar cell array. (d) Inductor ripple current of the dc–dc power converter.

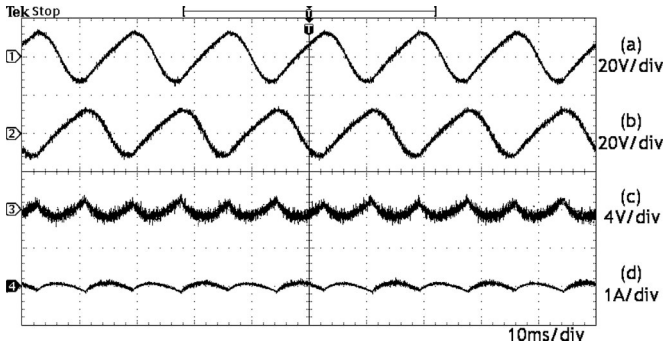

Fig. 15. Experimental results for the dc–dc power converter of the proposed transformerless grid-connected power converter. (a) Voltage ripple of capacitor C_2. (b) Voltage ripple of capacitor C_3. (c) Output voltage ripple of the solar cell array. (d) Inductor ripple current of the dc–dc power converter.

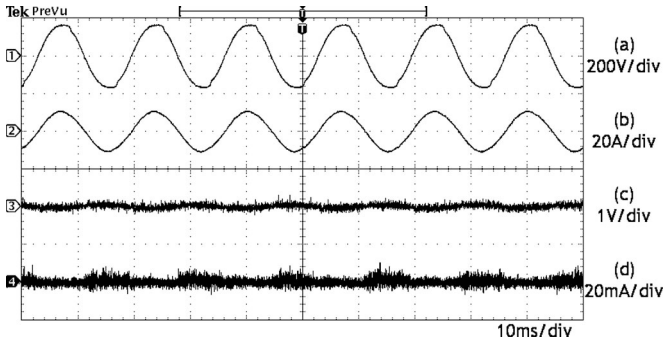

Fig. 16. Experimental results of the grounding voltage and the leakage current of the proposed transformerless grid-connected power converter. (a) Utility voltage. (b) Output current of the dc–ac inverter. (c) Voltage of the negative terminal of the solar cell array referred to the ground. (d) Leakage current.

is about 931 W. Fig. 13(b) shows that the output current of the dc–ac inverter is sinusoidal and in phase with the utility voltage. The total harmonic distortions (THDs) of the utility voltage and the output current of the dc–ac inverter are 4.0% and 2.5%, respectively. This verifies that the proposed transformerless grid-connected power converter can convert solar power to ac power with unity power factor. As seen in Fig. 13(c) and (d), both capacitor voltages V_{dc2} and V_{dc3} remain stable at 190 V.

Since the dc capacitors C_2 and C_3 perform the function of the energy buffer and are alternately charged and discharged for every half-cycle of the utility, both capacitor voltages V_{dc2} and V_{dc3} contain a 60-Hz voltage ripple. Fig. 14 shows the experimental results of the dc–dc power converter using a conventional voltage controller. As seen in Fig. 14(a) and (b), the peak-to-peak values of the voltage ripple at the capacitors C_2 and C_3 are about 28 V. Fig. 14(d) also shows that the inductor current of the dc–dc power converter still contains a significant current ripple. Therefore, the output voltage ripple of the solar cell array shown in Fig. 14(c) contains a voltage ripple, and the peak-to-peak value of the voltage ripple of the solar cell array is about 22 V. In this circumstance, the average output power of the solar cell array is about 890 W. Consequently, the voltage ripples in the dc capacitors C_2 and C_3 will pass to the output voltage of the solar cell array when the dc–dc power converter adopts a conventional voltage controller.

Fig. 15 shows the experimental results for the dc–dc power converter of the proposed transformerless grid-connected power converter. As seen in Fig. 15(a) and (b), the peak-to-peak value of the voltage ripple at the capacitors C_2 and C_3 is about 24 V. Fig. 15(d) shows that the ripple of an inductor current is very small due to the use of the current-mode control. In this way, the output voltage of the solar sell array can be sustained more stably. As seen in Fig. 15(c), the peak-to-peak value of the voltage ripple of the solar cell array is about 2.4 V and the average output power of the solar cell array is about 931 W. This verifies that the dc–dc power converter of the proposed transformerless grid-connected power converter can effectively suppress the voltage ripple of the solar cell array, yielding increased output power from the solar cell array. Comparing Figs. 14 and 15, it can be found that the voltage ripple of the solar cell array will reduce about 4% output power of the solar cell array.

Fig. 16 shows the experimental results of the grounding voltage and the leakage current of the proposed transformerless grid-connected power converter. A capacitor and a resistor are connected in series and then connected between the ground and the solar cell array to simulate the parasitic effect of the solar cell array. As seen in Fig. 16(c), the negative terminal voltage of the solar cell array with reference to the ground is about

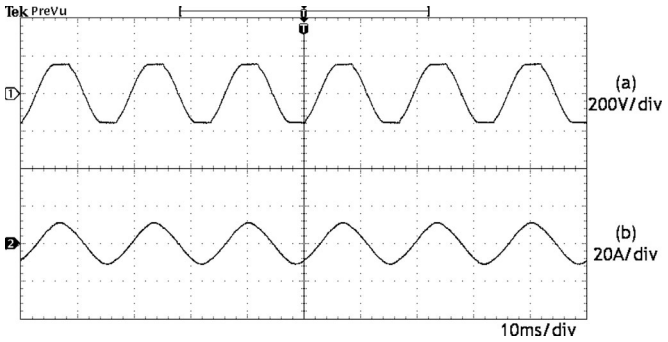

Fig. 17. Experimental results of the grid-connected power converter under the distorted utility voltage. (a) Utility voltage. (b) Output current of the dc–ac inverter.

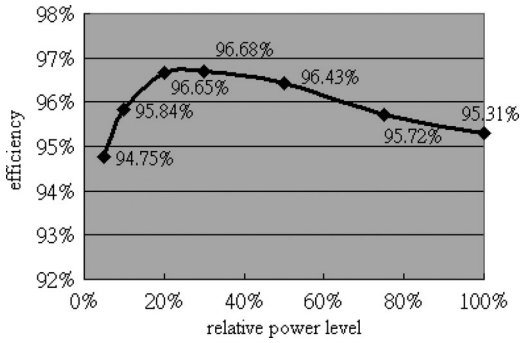

Fig. 18. Experimental results for the power efficiency of the grid-connected power converter under different output power.

0 V and contains nearly no high frequency component. The leakage current i_g, passing through the simulated capacitor and resistor, is shown in Fig. 16(d). It is smaller than 10 mA. Because of the small ripple for the negative terminal voltage of the proposed transformerless grid-connected power converter, the leakage current complies with the requirement stated in the VDE 0126-1-1 standard [25]. This effectively demonstrates that the proposed transformerless grid-connected power converter can not only solve the problem of TCO corrosion but also the problem of leakage current.

Fig. 17 shows the experimental results of the grid-connected power converter under the distorted utility voltage. The THD% of the distorted utility voltage shown in Fig. 17(a) is 7.5%. As seen in Fig. 17(b), the output current of the dc–ac inverter is still very close to sinusoidal. The THD% of output current of the dc–ac inverter is only 3.4%. This experiment verifies that the output current of the proposed grid-connected power converter can generate a sinusoidal output current even when the utility voltage is distorted.

Fig. 18 shows the experimental results for the power efficiency of the grid-connected power converter under different output powers. The solar cell array was replaced by a dc power supply to simplify the adjustment of output power in the experimental process. The output voltage of the dc power supply was set at 175 V. As can be seen, the power efficiency is 95.31% at full load and the maximum efficiency is 96.68%. The European efficiency is 96.17%.

VII. Conclusion

This paper proposes a novel transformerless grid-connected power converter. The negative terminal of the solar cell array can be directly connected to the ground in the proposed grid-connected power converter. The salient features of the proposed power converter are only two power electronic switches of the power converter are operated at high switching frequency simultaneously (one is a dc–dc power converter and the other is a dc–ac inverter), and the negative terminal of the solar cell array is directly connected to the ground to solve the problems of TCO corrosion and leakage current for some types of thin-film solar cell array. The experimental results show that the proposed grid-connected power converter can trace the maximum power point of the solar cell array, convert solar power to a high quality ac power to inject into the utility, and reduce the leakage current of the solar cell array.

Acknowledgment

The authors would like to thank ABLEREX Corporation, Ltd., Irwindale, CA, for the financial and technical support in this paper.

References

[1] T. Suntio, J. Leppaaho, J. Huusari, and L. Nousiainen, "Issues on solar-generator interfacing with current-fed MPP-tracking converters," *IEEE Trans. Power Electron.*, vol. 25, no. 9, pp. 2409–2419, Sep. 2010.

[2] S. L. Brunton, C. W. Rowley, S. R. Kulkarni, and C. Clarkson, "Maximum power point tracking for photovoltaic optimization using ripple-based extremum seeking control," *IEEE Trans. Power Electron.*, vol. 25, no. 10, pp. 2531–2540, Oct. 2010.

[3] L. Maharjan, S. Inoue, H. Akagi, and J. Asakura, "State-of-charge (SOC)-balancing control of a battery energy storage system based on a cascade PWM converter," *IEEE Trans. Power Electron.*, vol. 24, no. 6, pp. 1628–1636, Jun. 2009.

[4] J. M. A. Myrzik and M. Calais, "String and module integrated inverters for single-phase grid connected photovoltaic systems—a review," in *Proc. IEEE Bologna Power Tech Conf.*, Jun. 23–26, 2003, vol. 2, pp. 1–8.

[5] J. Leppaaho and T. Suntio, "Dynamic characteristics of current-fed super-buck converter," *IEEE Trans. Power Electron.*, vol. 26, no. 1, pp. 200–209, Jan. 2011.

[6] A. Koran, K. Sano, R. Y. Kim, and J. S. Lai, "Design of a photovoltaic simulator with a novel reference signal generator and two-stage LC output filter," *IEEE Trans. Power Electron.*, vol. 25, no. 5, pp. 1331–1338, May 2010.

[7] U. Boeke and H. van der Broeck, "Transformer-less converter concept for a grid-connection of thin-film photovoltaic modules," in *Proc. IEEE Ind. Appl. Soc. Annu. Meet.*, Oct. 5–9, 2008, pp. 1–8.

[8] Y. Sozer and D. A. Torrey, "Modeling and control of utility interactive inverters," *IEEE Trans. Power Electron.*, vol. 24, no. 11, pp. 2475–2483, Nov. 2009.

[9] Z. Liang, R. Guo, J. Li, and A. Q. Huang, "A high-efficiency PV module-integrated DC/DC converter for PV energy harvest in FREEDM systems," *IEEE Trans. Power Electron.*, vol. 26, no. 3, pp. 897–909, Mar. 2011.

[10] A. Chen, W. Wang, C. Du, and C. Zhang, "Single-phase hybrid clamped three-level inverter based photovoltaic generation system," in *Proc. IEEE Int. Symp. Power Electron. Distrib. Generation Syst.*, Jun. 16–18, 2010, pp. 635–638.

[11] X. Li and A. K. S. Bhat, "Analysis and design of high-frequency isolated dual-bridge series resonant DC/DC converter," *IEEE Trans. Power Electron.*, vol. 25, no. 4, pp. 850–862, Apr. 2010.

[12] J. I. Itoh and F. Hayashi, "Ripple current reduction of a fuel cell for a single-phase isolated converter using a DC active filter with a center tap," *IEEE Trans. Power Electron.*, vol. 25, no. 3, pp. 550–556, Mar. 2010.

[13] T. Kerekes, M. Liserre, R. Teodorescu, C. Klumpner, and M. Sumner, "Evaluation of three-phase transformerless photovoltaic inverter topologies," *IEEE Trans. Power Electron.*, vol. 24, no. 9, pp. 2202–2211, Sep. 2009.

[14] R. Gonzalez, J. Lopez, P. Sanchis, and L. Marroyo, "Transformerless inverter for single-phase photovoltaic systems," *IEEE Trans. Power Electron.*, vol. 22, no. 2, pp. 693–697, Mar. 2007.
[15] M. Calais and V. G. Agelidis, "Multilevel converters for single-phase grid connected photovoltaic systems-an overview," in *Proc. IEEE Int. Symp. Ind. Electron.*, Jul. 7–10, 1998, vol. 1, pp. 224–229.
[16] H. Schmidt, "Do thin-film modules need special inverters?" presented at the Fifth User Forum Thin-Film Photovoltaics, Würzburg, Germany, Jan. 26–28, 2009.
[17] C. R. Osterwald, T. J. McMahon, J. A. del Cueto, J. Adelstein, and J. Pruett, "Accelerated stress testing of thin-film modules with SnO_2 :F transparent conductors," in *Proc. National Center Photovoltaics Solar Program Rev. Meet.*, Mar. 24–26, 2003, pp. 1–4.
[18] S. V. Araujo, P. Zacharias, and B. Sahan, "Novel grid-connected non-isolated converters for photovoltaic systems with grounded generator," in *Proc. IEEE Power Electron. Spec. Conf.*, Jun. 15–19, 2008, pp. 58–65.
[19] L. Quan and P. Wolfs, "A review of the single phase photovoltaic module integrated converter topologies with three different DC link configurations," *IEEE Trans. Power Electron.*, vol. 23, no. 3, pp. 1320–1333, May 2008.
[20] O. Lopez, R. Teodorescu, and J. Doval-Gandoy, "Multilevel transformerless topologies for single-phase grid-connected converters," in *Proc. IEEE Conf. Ind. Electron.*, Nov. 6–10, 2006, pp. 5191–5196.
[21] L. Ma, T. Kerekes, R. Teodorescu, X. Jin, D. Floricau, and M. Liserre, "The high efficiency transformer-less PV inverter topologies derived from NPC topology," in *Proc. Eur. Conf. Power Electron. Appl.*, Sep. 8–10, 2009, pp. 1–10.
[22] W. Yu, J. S. Lai, H. Qian, C. Hutchens, J. Zhang, G. Lisi, A. Djabbari, G. Smith, and T. Hegarty, "High-efficiency inverter with H6-type configuration for photovoltaic non-isolated ac module applications," in *Proc. IEEE Appl. Power Electron. Conf. Expo.*, Mar. 18, 2010, pp. 1056–1061.
[23] H. Xiao and S. Xie, "Leakage current analytical model and application in single-phase transformerless photovoltaic grid-connected inverter," *IEEE Trans. Electromagn. Compat.*, vol. 52, no. 4, pp. 902–913, Nov. 2010.
[24] *IEEE Guide for Safety in AC Substation Grounding*, IEEE Standard 80-2000, Jan. 2000.
[25] *Automatic Disconnection Device Between a Generator and the Public Low-Voltage Grid*, Standard DIN VDE 0126-1-1, Feb. 2006.
[26] O. Lopez, F. D. Freijedo, A. G. Yepes, P. Fernandez-Comesaa, J. Malvar, R. Teodorescu, and J. Doval-Gandoy, "Eliminating ground current in a transformerless photovoltaic application," *IEEE Trans. Energy Convers.*, vol. 25, no. 1, pp. 140–147, Mar. 2010.
[27] H. L. Jou, K. D. Wu, J. C. Wu, and J. M. Shen, "Simplified maximum power point tracking method for the grid-connected wind power generation system," *Electr. Power Compon. Syst.*, vol. 36, no. 11, pp. 1208–1217, Nov. 1, 2008.
[28] T. J. Liang and J. L. Shyu, "Improved DSP-controlled online UPS system with high real output power," *IEE Proc. Electr. Power Appl.*, vol. 151, no. 1, pp. 121–127, Jan. 9, 2004.

Jia-Min Shen (S'08) was born in Tainan, Taiwan, in 1982. He received the M.S.E.E. degree from the National Kaohsiung University of Technology, Kaohsiung, Taiwan, in 2005. He is currently working toward the Ph.D. degree in electrical engineering from the National Kaohsiung University of Applied Sciences, Kaohsiung.

His research interests include power electronics applications and DSP control.

Hurng-Liahng Jou (M'99) was born in Taiwan in 1959. He received the B.S.E.E. degree from Chung Yuan University, Jonglih, Taiwan, in 1982, and the M.S.E.E and Ph.D.E.E. degrees from National Cheng Kung University, Tainan, Taiwan, in 1984 and 1991, respectively.

He is currently a Professor in the Department of Electrical Engineering, National Kaohsiung University of Applied Sciences, Kaohsiung, Taiwan. His research interests include power electronics applications and power quality improvement technique.

Jinn-Chang Wu (M'07) was born in Tainan, Taiwan, in 1968. He received the M.S.E.E. and Ph.D.E.E. degrees from National Cheng Kung University, Tainan, Taiwan, in 1992 and 2000, respectively.

He is currently an Associate Professor in the Department of Microelectronics Engineering, National Kaohsiung Marine University, Kaohsiung. His research interests include power quality and power electronics applications.